University of Groningen

Coulomb-blockade transport in single-crystal organic thin-film transistors

Schoonveld, W.A; Wildeman, J.; Fichou, D.; Bobbert, P.A.; Wees, B.J.van; Klapwijk, T.M

IMPORTANT NOTE: You are advised to consult the publisher's version (publisher's PDF) if you wish to cite from it. Please check the document version below.

Document Version
Publisher's PDF, also known as Version of record

Publication date:
2000

[Link to publication in University of Groningen/UMCG research database](#)

Coulomb-blockade transport in single-crystal organic thin-film transistors

W. A. Schoonveld*†, **J. Wildeman**†‡, **D. Fichou**§, **P. A. Bobbert**∥, **B. J. van Wees***† & **T. M. Klapwijk**¶

* *Department of Applied Physics,* † *Materials Science Center,* ‡ *Department of Polymer Chemistry, University of Groningen, Nijenborgh 4, 9747 AG Groningen, The Netherlands*

§ *Laboratoire des Matériaux Moléculaires, CNRS, 2 rue Henry-Dunant, 94320 Thiais, France*

∥ *Physics Department, Eindhoven University of Technology, PO Box 513, NL-5600 MB Eindhoven, The Netherlands*

¶ *Delft University of Technology, Department of Applied Physics, Nanophysics and Nanotechnology Section, Lorentzweg 1, 2628 CJ Delft, The Netherlands*

Coulomb-blockade transport—whereby the Coulomb interaction between electrons can prohibit their transport around a circuit—occurs in systems in which both the tunnel resistance, R_T, between neighbouring sites is large ($\gg h/e^2$) and the charging energy, E_C ($E_C = e^2/2C$, where C is the capacitance of the site), of an excess electron on a site is large compared to kT. (Here e is the charge of an electron, k is Boltzmann's constant, and h is Planck's constant.) The nature of the individual sites—metallic, superconducting, semiconducting or quantum dot—is to first order irrelevant for this phenomenon to be observed[1]. Coulomb blockade has also been observed in two-dimensional arrays of normal-metal tunnel junctions[2], but the relatively large capacitances of these micrometre-sized metal islands results in a small charging energy, and so the effect can be seen only at extremely low temperatures. Here we demonstrate that organic thin-film transistors based on highly ordered molecular materials can, to first order, also be considered as an array of sites separated by tunnel resistances. And as a result of the subnanometre sizes of the sites (the individual molecules), and hence their small capacitances, the charging energy dominates at room temperature. Conductivity measurements as a function of both gate bias and temperature reveal the presence of thermally activated transport, consistent with the conventional model of Coulomb blockade.

The experimental transport data available in the literature[3-8], obtained with highly ordered polycrystalline thin-film transistors (TFTs) based on α-6T and pentacene (see Fig. 1a), have so far been interpreted in terms of hopping between localized trap states, polaron hopping (both correlated and uncorrelated) or in terms of the Holstein model. However, large variations in the experimental data—on even nominally identical samples—limit the understanding of the intrinsic charge transport mechanisms of these systems.

Our sample layout is shown in Fig. 1a. The substrate is a highly doped silicon wafer, acting as a gate electrode, which is thermally oxidized in a dry atmosphere. The gold source and drain electrodes are lithographically defined, with gap diameters ranging from 2 to

20 μm. A second isolation layer is deposited to isolate the transistor electrically from neighbouring devices. The organic materials used were pentacene (Aldrich), quaterthiophene (α-4T; synthesized by Syncom BV) and sexithiophene (α-6T; also from Syncom BV). These materials were purified, and deposited in the last fabrication step by thermal evaporation in a high-vacuum environment (1×10^{-7} mbar). Large individual crystallites within a polycrystalline thin film are obtained by optimization of the substrate temperature and evaporation rate[9,10]. With optimal settings the individual crystallites can grow up to 40 μm in diameter, which is large enough to fill one gap completely, resulting in a single-crystal TFT[11]. The identification, orientation and thickness of the single crystals can be obtained by an optical polarization microscopy technique[9].

Room-temperature current–voltage (I–V) characteristics of a crystal pentacene TFT with a thin-film phase[10], measured with increasing and decreasing drain voltage, are shown in Fig. 2a. All measurements are performed under high-vacuum conditions, and as a result show little or no hysteresis in the drain voltage sweep. In contrast to what is generally reported in the literature, we typically observe non-ohmic behaviour of the gold source and drain contacts to the organic active layer[11], as is demonstrated at low drain bias in Fig. 2. The conductivity is obtained in the linear transport regime as a function of gate bias[12], and corrected for the non-ohmic contacts. A typical result is shown in Fig. 2b. The non-ohmic effects of the contacts were compensated for by measuring several sweeps of gate voltage with increasing source–drain bias ($V_d = -4, -5, -6$ and -7 V). The channel conductance at a set gate voltage is then obtained from the slope of the channel current with the applied
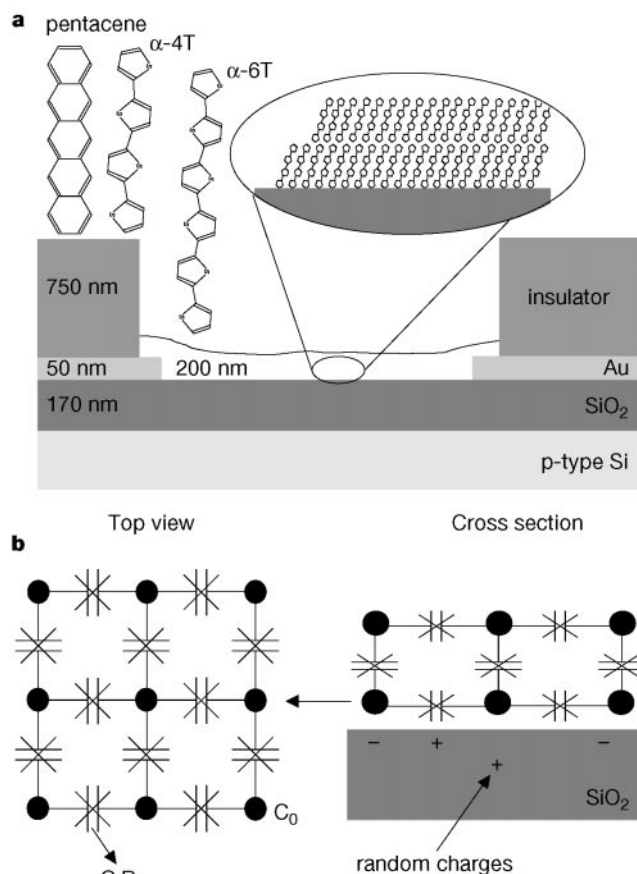
Figure 1 Schematic sample layout. **a**, Single-crystal TFT sample structure for α-4T, α-6T and pentacene materials. **b**, A schematic view of two molecular layers on top of the SiO₂ gate-dielectric with random charges incorporated. In the in-plane direction, the layers are represented by a two-dimensional array of molecules separated by a tunnel junction resistance R_T with nearest-neighbour capacitance C. The self-capacitance molecule is given by C_0.

drain voltage. This procedure is applied to all measured gate voltages, enabling the channel conductance to be obtained as a function of gate voltage.

The resulting charge transport data of the pentacene TFT are shown in Fig. 3. The channel conductivity is clearly thermally activated, with a gate-voltage-dependent activation energy (Fig. 3a and c). Similar behaviour of the activation energy has been reported[13] for organic TFTs with an amorphous active layer. In this case the transport has been described by a variable-range hopping process between localized trap states.

We found that the extrapolated conductivity σ_0 at high temperatures shows a linear dependence on gate voltage (Fig. 3b) and vanishes at a threshold voltage of $V_t = +9.6\,V$. This threshold voltage marks the onset for p-type conduction in pentacene TFTs, and is a crucial value needed to calculate the actual charge carrier density n_s in the active layer. Note that this value contrasts sharply with the 'threshold voltage', which might be extracted from the quasi-linear regime of the channel conductance with gate voltage (Fig. 2b). The threshold voltage obtained in this fashion is in our view not relevant to the calculation of the effective charge carrier density, as no real onset for conduction can be discriminated.

The transport data are interpreted in terms of the Coulomb-blockade model in the orthodox regime, in which the tunnel resistance between neighbouring sites is larger than the quantum resistance ($R_T \gg R_Q = h/e^2 \approx 25\,k\Omega$)[1]. In a first-order approximation, we will assume a metallic-like behaviour of the molecular islands. Note however that, in contrast to metallic islands, the level spacing δE in molecules is generally larger than kT. With this relatively large level spacing the bandwidth Γ, which is given by the product of the transmission probability and the energy level spacing[14] $\Gamma \equiv |t|^2 \delta E$, could become large enough to break down the regime of the orthodox Coulomb blockade.

Transport in the orthodox regime is described by tunnelling of localized charges between nearest-neighbour islands, driven by the energy difference between the initial and final energy states. The charging energy of a site can be approximated by:

$$E_C = \frac{(ne - Q_{ind})^2}{2C} \qquad (1)$$

where Q_{ind} is the induced charge on a molecule, and n the number of charge carriers on the molecule. The induced charge Q_{ind} can have

non-integer values because of the random offset charges present in the SiO_2 dielectric layer (Fig. 1b). Alternatively, positional disorder of the molecules can give rise to different nearest-neighbour capacitances, which also affects the charging energy (equation (1)). The maximum energy barrier between neighbouring sites can be estimated by the charging energy at the degeneracy point at which the induced charge on the dot is equal to a half-filling $Q_{ind} = e(n \pm 1/2)$ (equation (1)).

It follows that the observed energy barrier is a product of the charging energy and the induced random offset charges. The charging energy of a molecule is of the order of $E_C = e^2/2C \approx 1\,eV$ and the typically observed activation energies are roughly 0.1 eV, from which we estimate the maximum induced charge on a molecule to be about 10% of an electron charge. The transport is then probably dominated by activated hops between nearest-neighbour sites, with an energy barrier dependent on the charge carrier density. We suggest that the conductivity can be described by:

$$\sigma(n_s, T) = \sigma_0 \exp\left(-\frac{E_{act}(n_s) + E_p}{kT}\right) \qquad (2)$$

with $\sigma_0 = n_s e \mu_0$ the high-temperature conductivity, and μ_0 the intrinsic mobility determined by $\mu_0 = (R_T n_{sites} e)^{-1}$ with R_T an energy independent tunnel resistance. (The number of available sites n_{sites} is obtained from single crystal X-ray diffraction data[15–17]
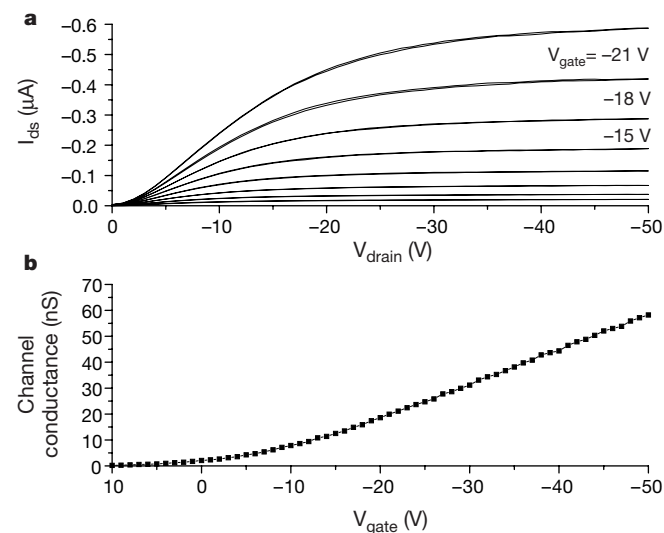
Figure 2 Room-temperature current–voltage characteristics of a single-crystal pentacene TFT with gap length of 8 μm and width of 16 μm. **a**, Standard TFT characteristics, showing the linear and saturation regimes. Note the gradual onset at low drain bias which is due to non-ohmic contacts. **b**, The channel conductance as a function of gate bias. The data have been corrected for the non-ohmic contacts.

Figure 3 Charge transport data of the pentacene TFT shown in Fig. 2. **a**, The conductivity shows thermally activated behaviour over the entire gate voltage range. **b**, The extrapolated conductivity σ_0 at $T \to \infty$ increases linearly with gate voltage. The threshold voltage V_t marks the onset of p-type conduction for pentacene TFTs. **c**, The resulting activation energy as a function of gate voltage. The error bars are representative of the I–V measurement accuracy.

and is given in Table 1), n_s the charge carrier density, E_{act} the activation energy and E_p a possible polaron binding energy term. The orthodox Coulomb-blockade description assumes that the intermediate microscopic processes, such as the details of the tunnelling and relaxation processes once the charge has tunnelled, can in first order be neglected (this requires the polaron relaxation time, Δt, to be $< \hbar/E_p$). Note that this contrasts with the polaron hopping theories[18,19], in which the microscopic details of the hopping motion of the charges are relevant for the charge transport mechanism. The activation energy is dependent on the charge carrier density and the magnitude is determined by the charging energy together with the random offset charges. However, we also allow for a n_s-independent energy term E_p that takes into account a possible contribution from polarons to the transport if the polaron relaxation time Δt exceeds $\Delta t > \hbar/E_p \approx 10^{-13}$ s. We note that this term is independent of the charge carrier density. The extrapolated tunnel resistance should be larger than the quantum resistance to be consistent with the model just described. We therefore associate with the quantum resistance a 'critical' mobility $\mu_c = e/(n_{sites}h)$ which marks the boundary between thermally activated and temperature-independent transport if the intrinsic mobility is smaller ($\mu_0 \ll \mu_c$) or larger ($\mu_0 \gg \mu_c$) than the critical mobility.

The temperature dependent data of α-4T and α-6T single-crystal TFTs show a similar behaviour of the extrapolated conductivity and activation energy as a function of charge carrier density as the pentacene data already shown (Fig. 4). The transport processes of these highly ordered materials appear to be very similar, and show a strong dependence on the size of the molecule, which confirms the arguments of the orthodox Coulomb-blockade model.

In Table 1 we give the relevant parameters for the different materials. The tunnel barriers for these materials are indeed sufficiently large to be in the orthodox regime ($R_T \gg R_Q$). Note that the values of the intrinsic mobility μ_0 are smaller than the 'critical' mobility μ_c.

The threshold voltages in Table 1 are representative for the onset of p-type conduction for the different materials. The differences between the obsrved threshold voltage values are probably related to the work-function differences between the materials. However, the work-function difference between α-4T and α-6T is about 0.5 V (S. C. Veenstra et al., manuscript in preparation), which is substantially smaller than the observed threshold voltage difference of 3.0 V. The exact origin of this effect is not understood. The listed values for the charging energies are rough estimates obtained from the maximum activation energy with an assumed number of random offset charges corresponding to an induced charge of $0.5e$ on the molecule. Alternatively, the charging energy can be calculated based on the self-capacitance of a α-4T molecule (assuming a sphere of radius r ($r = 16.4/2$ Å) the capacitance is about $C \approx 9 \times 10^{-19}$ F) which results in $E_C \approx 0.9$ eV.

All TFTs were fabricated using identical SiO_2 gate dielectric, and therefore we assume that the number of random offset charges in the SiO_2 is constant for all three materials. The observed activation energies should then directly scale with the charging energies and thus the capacitances of the molecules used, which to a first approximation is determined by their geometrical dimensions. This is demonstrated by the dependence of the observed activation

energies on charge carrier density. The scaling of the activation energies at identical charge carrier densities for α-4T and α-6T yields a constant value of 2, which can roughly be compared to a factor of 1.5 obtained with the self-capacitance (using the length) of both molecules. To improve the correspondence between both values, a more detailed approximation of the molecular capacitance, in which the actual charge distribution in relation to the nature and number of the charge carriers on the molecule, has to be taken into account. The activation energies do not tend to saturate at high carrier densities (see Fig. 4), which in our view confirms that polaron effects do not dominate transport.

We have performed numerical calculations in the orthodox regime, based on a two-dimensional array of 16×16 sites[20,21], similar to Fig. 1b, in which the dynamic properties are described by single-electron processes. A thermally activated transport behaviour is observed with activation energies dependent on charge carrier density. The magnitude is determined by the charging energy and number of random offset charges (data points in Fig. 4b). The simulations confirm that the extrapolation to infinite temperatures indeed yields the nearest-neighbour tunnel resistance. More detailed calculations of the molecular capacitance and the array need to be done in order to tighten the comparison with experiments.

The conductivity of organic TFTs is thus the result of an interplay between the intrinsic nearest-neighbour tunnel resistance and the capacitance of the individual molecules. Molecules with a higher capacitance will result in a lower activation energy and an increased conductivity. An alternative, more appealing, route to obtain organic materials with a high intrinsic mobility for device applications would be to decrease the tunnel resistance to the order of , or lower than, the quantum resistance (which is almost the case for α-4T). In such a regime, the orthodox Coulomb-blockade model breaks down, and charging effects will cease to play a role in transport, which would lead to high, temperature-independent mobilities ($\mu_0 > 0.5$ cm^2 V^{-1} s^{-1}). □

Figure 4 Comparison of the charge transport data of α-4T, α-6T and pentacene. **a**, The extrapolated conductivity σ_0, and **b**, the activation energy, as a function of charge carrier density. The activation obtained from numerical simulations are plotted (diamonds) for carrier densities of 1, 2 and 4 charges in the two-dimensional array with $E_C = 0.4$ eV and random charges of 0.1 e.

Table 1 Charge transport parameters of α-4T, α-6T and pentacene TFTs

Parameter	Material		
	α-4T	α-6T	Pentacene
V_t (V)	+2.0	+5.0	+9.6
n_{sites} (10^{18} m^{-2})	4.18	4.23	4.15
R_T (kΩ)	64	106	250
E_C (eV)	0.8	0.6	0.4
μ_0 (10^{-1} cm^2 V^{-1} s^{-1})	2.3	1.4	0.6
μ_c (10^{-1} cm^2 V^{-1} s^{-1})	5.8	5.7	5.8

1. Grabert, H. & Devoret, M. H. in *Single Charge Tunneling* (eds Grabert, H. & Devoret, M. H.) Ch. 1 (NATO ASI Ser., Plenum, New York, 1992).

2. Mooij, J. E. *et al.* Unbinding of charge-anticharge pairs in 2-dimensional arrays of small tunnel-junctions. *Phys. Rev. Lett.* **65**, 645–649 (1990).

3. Horowitz, G., Hajlaoui, R. & Delannoy, P. Temperature-dependence of the field-effect mobility of sexithiophene—determination of the density of traps. *J. Phys. III* **5**, 355–371 (1995).

4. Nelson, S. F., Lin, Y.-Y., Gundlach, D. J. & Jackson, T. N. Temperature-independent transport in high-mobility pentacene transistors. *Appl. Phys. Lett.* **72**, 1854–1856 (1998).

5. Schön, J. H. & Batlogg, B. Modeling of the temperature dependence of the field-effect mobility in thin film devices of conjugated oligomers. *Appl. Phys. Lett.* **74**, 260–262 (1999).

6. Waragai, K., Akimichi, H., Hotta, S. & Kano, H. Charge transport in thin-films of semiconducting oligothiophenes. *Phys. Rev. B* **52**, 1786–1792 (1995).

7. Torsi, L., Dodabalapur, A., Rothberg, L. J., Fung, A. W. P. & Katz, H. E. Intrinsic transport properties and performance limits of organic field-effect transistors. *Science* **272**, 1462–1464 (1996).

8. Torsi, L., Dodabalapur, A., Rothberg, L. J., Fung, A. W. P. & Katz, H. E. Charge transport in oligothiophene field-effect transistors. *Phys. Rev. B* **57**, 2271–2275 (1998).

9. Vrijmoeth, J., Stok, R. W., Veldman, R., Schoonveld, W. A. & Klapwijk, T. M. Single crystallites in "planar polycrystalline" oligothiophene films: Determination of orientation and thickness by polarization microscopy. *J. Appl. Phys.* **83**, 3816–3824 (1998).

10. Bouchoms, I. P. M., Schoonveld, W. A., Vrijmoeth, J. & Klapwijk, T. M. Morphology identification of the thin film phases of vacuum evaporated pentacene on SiO$_2$ substrates. *Synth. Met.* **104**, 175–178 (1999).

11. Schoonveld, W. A., Vrijmoeth, J. & Klapwijk, T. M. Intrinsic charge transport properties of an organic single crystal determined using a multiterminal thin-film transistor. *Appl. Phys. Lett.* **73**, 3884–3886 (1998).

12. Brown, A. R., Jarrett, C. P., De Leeuw, D. M. & Matters, M. Field-effect transistors made from solution-processed organic semiconductors. *Synth. Met.* **88**, 37–55 (1997).

13. Vissenberg, M. C. J. M. & Matters, M. Theory of the field-effect mobility in amorphous organic transistors. *Phys. Rev. B* **57**, 12964–12967 (1998).

14. Schoeler, H. in *Mesoscopic Electron Transport* (eds Sohn, L. L., Kouwenhoven, L. P. & Schön, G.) Ch. 1 (NATO ASI Ser., Kluwer Academic, Dordrecht, 1997).

15. Porzio, W., Destri, S., Mascherpa, M. & Brückner, S. Structural aspects of oligothienyl series from X-ray-powder diffraction data. *Acta. Polymer.* **44**, 266–272 (1993).

16. Horowitz, G. *et al.* Growth and characterization of sexithiophene single-crystals. *Chem. Mater.* **7**, 1337–1341 (1995).

17. Campbell, R. B., Robertson, J. M. & Trotter, J. The crystal structure of hexacene, and a revision of the crystallographic data for tetracene. *Acta Crystallogr.* **15**, 289–299 (1962).

18. Holstein, T. Studies of polaron motion Part I. The molecular-crystal model. *Ann. Phys.* **8**, 325–387 (1959).

19. Silinsh, E. A. & Cápek, V. *Organic Molecular Crystals* (AIP Press, New York, 1994).

20. Geigenmüller, U. & Schön, G. Single-electron effects in arrays of normal tunnel-junctions. *Europhys. Lett.* **10**, 765–770 (1989).

21. Bobbert, P. A., Geigenmüller, U., Fazio, R. & Schön, G. in *Macroscopic Quantum Phenomena* (eds Clark, T. *et al.*) 119–122 (World Scientific, New York, 1990).

•••

Inorganic yellow-red pigments without toxic metals

M. Jansen* & H. P. Letschert†

* *Max-Planck-Institut für Festkörperforschung, Heisenbergstrasse 1, D-70569 Stuttgart, Germany*
† *dmc², Degussa Metals Catalysts Cerdec, Postfach 11 04 03, D-60039 Frankfurt am Main, Germany*

....

Inorganic pigments have been utilized by mankind since ancient times[1], and are still widely used to colour materials exposed to elevated temperatures during processing or application[2]. Indeed, in the case of glasses, glazes and ceramics, there is no alternative to inorganic pigments for colouring. However, most inorganic pigments contain heavy metals or transition metals that can adversely effect the environment and human health if critical levels are exceeded. Cadmium-based pigments in particular are a cause of concern[3]: although the pigments are not toxic due to their very low solubility in water and dilute mineral acids, cadmium itself is toxic and can enter the environment in a bioavailable form through waste-disposal sites and incineration plants[4]. This has led to regulations, based on the precautionary principle, that strongly restrict the use of cadmium pigments[5]. And even though recent assessments[20,21] have concluded that the risk to humans or the environment might be not as significant as originally feared, a strong demand for inherently safer substitutes remains. Here we demonstrate that solid solutions of the perovskites CaTaO$_2$N and LaTaON$_2$ constitute promising candidates for such substitutes: their brilliance, tinting strength, opacity, dispersability, light-fastness and heat stability rival that of the cadmium pigments, while their colour can be tuned through the desired range, from yellow through orange to deep red, by simple composition adjustments. Because all the constituent elements are harmless, this perovskite-based inorganic pigment system seems a promising replacement that could eliminate one of the sources for cadmium emissions to the environment and some of the remaining concerns about pigment safety.

In general, colours of solids appear brilliant and pure when the corresponding mechanism for a selective absorption of light is related to an electronic interband transition, leading to a steep absorption edge in the visible spectrum. The width of the bandgap is determined by the extent of overlap of the valence orbitals, and by the difference between the electronegativities of the cations and anions involved. A concept[6,7] has been derived from these factors (that is, valence-orbital overlap and electronegativity difference) that allows *a priori* design of bandgaps in semiconductors. In trying to rationally develop new inorganic pigments, we have adopted these ideas, mainly focusing on the option of widening the bandgap by increasing the difference of electronegativities between the respective cationic and anionic elements, and vice versa. Because we study optical effects, we have preferred to use the so-called optical electronegativities[8]. Whereas the electronegativities of the metals only vary in small steps, the substitution of one non-metal by another usually produces large shifts in electronegativity difference. Thus, in order to achieve a fine-tuning of bandgaps, we have focused on materials containing two different non-metals. For such compounds, the weighted average of the electronegativities of the respective anions has proved to be a good first approximation[6,7].

Table 1 Colour data of (Ca, La)Ta(O, N)$_3$ and of some commercial pigments

System	L^*	a^*	b^*
Ca$_{(1-x)}$La$_x$TaO$_{(2-x)}$N$_{(1+x)}$			
$x = 0.05$	77.70	−7.07	83.86
$x = 0.15$	62.34	9.82	80.50
$x = 0.3$	59.20	22.91	78.79
$x = 0.45$	52.16	28.64	73.58
$x = 0.6$	47.60	37.26	67.00
$x = 0.75$	35.21	42.35	55.71
$x = 0.9$	31.62	49.29	39.29
$x = 1.0$	26.35	37.01	30.08
Cadmium yellow	75.66	−7.90	99.12
Cadmium orange	64.68	47.70	96.26
Cadmium red	41.10	65.21	56.84
Cadmium dark Red	28.06	56.11	35.29
Fe$_2$O$_3$	39.71	26.33	16.86
(Al$_{0.95}$Mn$_{0.05}$)$_2$O$_3$	22.83	19.14	15.38

Shown are the colour coordinates of Ca$_{(1-x)}$La$_x$TaO$_{(2-x)}$N$_{(1+x)}$, $x = 0.05 − 1.0$, of four cadmium sulphoselenides and of two commercial red pigments without toxic metals. CIELab colour coordinates (L^* = brightness axis, maximum values: 100 = white, 0 = black; a^* = green-red axis, negative direction = green, positive direction = red; b^* = blue-yellow axis, negative direction = blue, positive direction = yellow) determined according to DIN 5033, Part 3, 1976, 2° Observer, Illuminant C, 26% pigment in PVC. Commercial cadmium-yellow (Product No. 16308), -orange (Product No. 16309), -red (Product No. 18373), -dark red (Product No. 16176) from producer James M. Brown Limited, Stoke-on-Trent ST4 4NX, UK. Fe$_2$O$_3$ (Product No. RD101) and (Al$_{0.95}$Mn$_{0.05}$)$_2$O$_3$ (Product No. FLO 172/411) from dmc² AG, Frankfurt/Main, Germany.